Journal of Structural Geology, Vol. 15, No. 12, pp. 1485 to 1495, 1993
Printed in Great Britain

0191-8141/93 $06.00 + 0.00

A comparison of seismic and structural measurements of scaling exponents during tensile subcritical crack growth

C. G. HATTON and I. G. MAIN

Department of Geology and Geophysics, University of Edinburgh, West Mains Road, Edinburgh EH9 3JW, U.K.

and

P. G. MEREDITH

Department of Geological Science, University College London, Gower Street, London WC1E 6BT, U.K.

(*Received* 12 *May* 1992; *accepted in revised form* 13 *November* 1992)

Abstract—The observed fractal nature of both fault length distributions and earthquake magnitude–frequency distributions suggests that there may be a relationship between the structure of active fault systems and the resulting seismicity. In previous theoretical work, a positive correlation between the exponent D from the fracture length distribution, and the seismic or acoustic emission (AE) b-value has been inferred from a simple dislocation model of the seismic source. Here, we present the first experimental evidence for a correlation between D and b from a series of tensile fracture mechanics tests on crystalline rock, carried out in different environmental conditions, both air-dry and water-saturated, and at ambient temperature and pressure. The microseismic acoustic emissions were monitored during subcritical crack growth under controlled conditions of constant stress intensity, K_I, and quantitative analyses of the resulting fracture patterns were carried out on the same specimens. It is found that AE b-values, ranging from 1.0 to 2.3, correlate negatively with the normalized stress intensity K_I/K_{IC}, where K_{IC} is the fracture toughness of the specimen. The microcrack length distribution exponent D, ranges from 1.0 to 1.7. Fluid presence has a first-order influence on both the AE and structure produced in these experiments. For experiments at low stress intensity or high fluid content, the activation of the stress corrosion mechanism for $K_I < K_{IC}$ leads to a greater relative proportion both of small cracks and of low amplitude acoustic emissions, reflected in higher values of D and b. The exponent D is found to correlate positively with the AE b-value.

INTRODUCTION

THE principle of self-similarity, or an appearance of identical features at different scales, has long been of fundamental importance in structural geology. Mandelbrot (1982) coined the term 'fractal' to describe such self-similar objects, and described various methods of measuring different fractal dimensions, each of which measure a different aspect of the self-similarity. More recently Turcotte (1989, 1992) defined a fractal set as any geometrical set which exhibits a power-law relationship: if a system is in some sense scale invariant, and the number of objects N with a characteristic size (or length) greater than L satisfies the relation:

$$N \sim L^{-D} \tag{1}$$

then D is a 'fractal' dimension, in the general sense of the term. This follows because the only distribution which is scale-invariant is a power law.

For example, Fig. 1(a) shows the length–frequency distribution of surface faults which have been shown by structural mapping to have been active in the Holocene in the conterminous United States (after Shaw & Gartner 1986), in the form of a power-law relation with a fractal dimension D equal to the negative slope of the straight line (D = 1.76 for this example). Figure 1(b) shows the log-linear magnitude–frequency distribution of earthquakes in southern California (after Main & Burton 1986). The slope in this case, referred to as the seismic b-value, can be shown to be proportional to the fractal dimension inferred from a simple dislocation model of the seismic source (Aki 1981, King 1983, Main & Burton 1984). Usually this relation takes the form:

$$D = \frac{3b}{c}, \tag{2}$$

where c is a constant that is usually found to be 3/2 (Kanamori & Anderson 1975).

It is important to establish the nature of this relationship experimentally, since much theoretical work on the evolution of fault and fracture systems is based on what has been up to now an inferred positive correlation between the length–frequency and the magnitude–frequency exponents indicated by the slopes of Fig. 1. Examples include the modelling of compressional failure of rock specimens in the laboratory (Main *et al.* 1990, Meredith *et al.* 1990) and the effect of the growth of fault populations on overall strain (Walsh & Watterson 1992). The argument in these models is that fault populations develop in increments which must at some timescale be linked to that of recorded earthquake populations. Thus the eventual fault pattern (Fig. 1a) is the

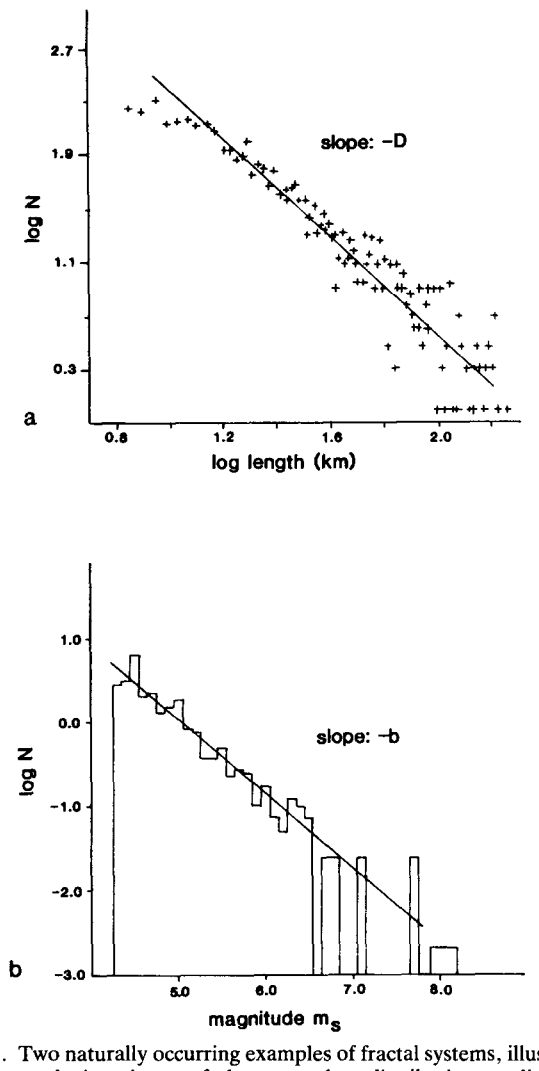

Fig. 1. Two naturally occurring examples of fractal systems, illustrating the scale invariance of the power-law distribution applied to structure and seismicity. (a) Discrete length–frequency distribution of active surface faults in the United States (after Shaw & Gartner 1986). This data gives a power-law distribution of fault lengths, with a fractional dimension of $D = 1.76$ from the negative slope of the best-fit straight line. (b) Discrete magnitude–frequency distribution of earthquakes in southern California (after Main & Burton 1986). This data also fit a straight-line power-law distribution, where the negative slope gives the seismic b-value. The similarity of the plots from these two examples indicates that there may be a direct relationship between structure and seismicity.

result of an integrated sequence of seismic increments on a smaller time-scale (Fig. 1b). This problem of relating posthumous geological structure to incremental seismic damage was addressed in Main *et al.* (1990), who concluded that the time-integrated fractal dimension of the fracture pattern (its length distribution exponent D) would tend to lag (be higher than) that of the incremental seismic population in the compressional tests described in their work. Also the nature of the scaling of fault dimensions is one of the main areas of current debate in establishing how fault or crack populations grow (Marrett & Allmendinger 1990, 1991, Scholz & Cowie 1990, Walsh *et al.* 1991, Cowie & Scholz 1992a,b). However, all of these arguments cloud the fact that even the basic correlation of the scaling properties of structural and seismic data for a single time increment has not up to now been established in the literature.

It is the purpose of this paper to present some new experimental data from a series of tensile fracture mechanics tests using the double torsion technique (Williams & Evans 1973), where microseismic acoustic emissions were monitored during subcritical crack growth under conditions of controlled constant rupture velocity, and where for the first time quantitative structural analyses of the resulting fracture patterns (involving the microfracture length distributions), have also been carried out on the same specimens. We have chosen subcritical crack growth by the mechanism of stress corrosion since this process is known to produce a large range of b-values depending on the presence of an active pore fluid and the rate of crack growth (Meredith *et al.* 1990), and is now thought to be a significant mechanism in rock fracture in the Earth (Anderson & Grew 1977, Das & Scholz 1981, Kerrich *et al.* 1981, Atkinson 1982, Etheridge 1983, Segall & Pollard 1983). Its chief advantage is that under experimental conditions the controlling variables, i.e. stress intensity and chemical environment, can be controlled to give accessible seismic and structural results in a reasonable time-scale. Each experiment represents a single time increment in the fault growth and fracture evolution models discussed above, and the scaling hypothesis between b and D can be tested objectively, without any need to assume a particular model.

In this paper we will quantify both the acoustic emission results and the structural geometry of the fracture system from each individual test specimen, in order to attempt to establish a direct relationship between the AE b-value and the scaling exponent D, and to use these quantitative parameters to examine the effects of fluid presence and crack velocity on tensile fracture.

EXPERIMENTAL METHOD

Overview

The experimental method chosen for this study was the double torsion test, whose specimen and loading geometry are described in Meredith & Atkinson (1985). This method has several advantages over other methods of tensile testing. The stress intensity is independent of crack length over much of the specimen length, the value of the stress intensity factor (K_I) is directly proportional to the applied load, and the crack velocity is related to the stress intensity. Although a stress gradient is present between the two surfaces of the specimen, the surface considered in our analysis was the undersurface that experiences tension. Since there is a stress gradient, it is most likely that cracks will propagate in the region of maximum tension, and so the undersurface should contain the majority of the cracks. A detailed discussion of the experimental technique is also given in Meredith & Atkinson (1985) and so is not repeated here.

In the present work, our main objective is to relate the crack growth and associated seismicity to the resulting structure of the cracks produced. Therefore, we have

chosen to use the constant displacement rate technique in order to apply uniform conditions of load and stress intensity over as much of the specimen volume as possible. This optimizes the specimen area amenable to uniform structural analysis, at the expense of having fewer results per test.

In this method, the load P is applied to the specimen at a constant displacement rate. The load is seen to increase approximately linearly until a critical load is reached and crack growth begins. The increasing displacement is then exactly compensated for in this loading geometry by the change in specimen compliance due to cracking, and the load in theory remains constant until failure. It is this constant loading criterion over much of the specimen that is important to this study. However, it is often difficult to achieve in practice. Figure 2 shows a typical load vs time plot. This illustrates both the degree of fluctuation inevitably involved due to the digital recording equipment (when the specimen is behaving linear-elastically between the origin and a), and also the additional fluctuation due to episodic crack growth (between a and b). An average load is taken to represent the 'constant' load during the time interval between (a) and (b) for each test. Typical standard deviations from the average load are of the order ± 10–25 N, compared with typical mean loads of 200–250 N.

This method of the double torsion test also has the advantage, specifically for this study, that the specimen is essentially a two-dimensional plate whose undersurface may be polished, thereby allowing direct inspection of the microfracture system produced around the growing macrocrack. This also obviates the need for sectioning, which in itself may introduce artificial damage. A constant stress intensity is achieved in the middle third of the specimen to a good approximation.

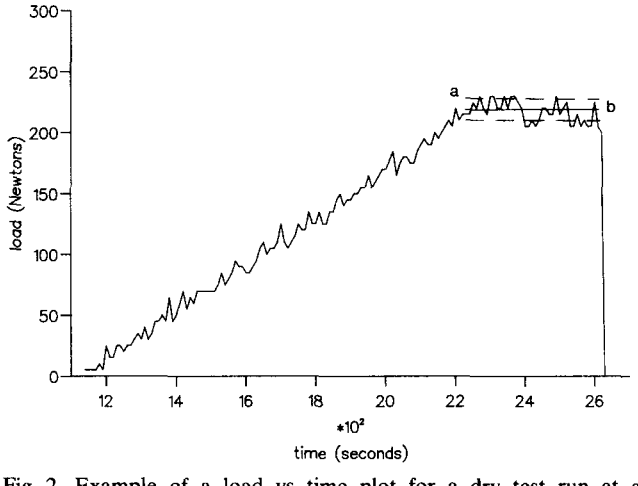

Fig. 2. Example of a load vs time plot for a dry test run at a displacement rate of 0.16×10^{-6} m s^{-1}. The load increases as the specimen shows linear-elastic behaviour, until microcracking begins at a. This coincides with the main onset of acoustic emission. The increasing ram displacement is then exactly compensated by the change in specimen compliance due to crack extension. The load then remains essentially constant (the straight line represents the arithmetic mean) until failure at b. From this plot, fluctuations in applied load are evident, thus introducing an inevitable error into subsequent calculations (the dashed lines represent the standard deviations from the mean, between a and b).

Theoretically, for mode I tensile fracture, the stress intensity factor K, a measure of the stress concentration at the crack tip, for this loading geometry is:

$$K_I = PW_m\left[\frac{3(1+\nu)}{Wd_n d^3\beta}\right]^{0.5}, \quad (3)$$

where P is the applied load, ν is Poisson's ratio, β is a dimensionless correction for the finite specimen width (Williams & Evans 1973, Fuller 1979) and the other parameters depend on the specimen geometry (W is the width of the specimen, W_m is the semi-moment arm—the distance between adjacent specimen support and loading point—d is the thickness and d_n is the thickness within the guide groove). The stress intensity is found experimentally to be related to the rupture velocity (Charles 1958, Atkinson 1987). Thus, a constant stress intensity also corresponds to a constant rupture velocity.

Test materials and specimen preparation

The crystalline rock type used in this experimental programme was the Loch Uisg microgranodiorite of Tertiary age from south Mull, northwest Scotland. In order to reduce the number of controlled variables to a minimum, the test specimens were obtained from field exposure of relatively unaltered, fine-grained igneous rock with no evident tectonic fabric and no visible pre-existing small-scale fractures or joints, in hand specimen or thin section.

The samples of Loch Uisg microgranodiorite were collected from an exposure on the south eastern shore of Loch Buie (grid reference: NM 6223). The rock consists of acicular augite, now altered to chlorite, plagioclase (albite) and orthoclase, in a micrographic groundmass containing only a small proportion of quartz. The average grain size is <0.5 mm, with phenocrysts of up to 1 mm. In our experiments the specimen thickness is 3–4 times the typical grain size, i.e. approximately 5 mm. The constraints of the loading geometry then require a specimen width of 60 mm and length of 150 mm (Meredith 1983).

The specimen has a guide groove for the main crack that is set upward, and a starting notch to provide an initial stress concentration to initiate crack propagation.

Summary of experimental procedure

During each test the controlling variables were loading ram displacement rate and fluid presence. The displacement rate controls the magnitude of the steady-state load P, and hence the stress intensity and average rupture velocity. Displacement rates varied between 0.016×10^{-6} and 5×10^{-6} m s^{-1}, and were maintained constant by servo-control. The longest experiment, running at the lowest displacement rate possible with the present equipment, ran for 6 h and the shortest ran for 70 s. 'Air-dry' tests with no fluid present at the crack tip were run in air at ambient humidity. 'Wet' tests were carried out with the specimens totally immersed in a

bath of de-ionized H_2O. One 'damp' test was carried out by pre-soaking the specimen in water and sponging water onto the specimen during the test merely to examine an intermediate case. The tests were carried out under ambient conditions of pressure and temperature.

Acoustic emissions, monitored with a single transducer, were logged continuously during each test. After the experimental run, the middle third of the polished undersurface of each specimen was analysed for evidence of both a macrofracture and subsidiary microcracking. The analysis of these seismic and structural properties are described in the following two sections.

ANALYSIS OF SEISMICITY

Acoustic emission recording

The acoustic emissions (AE) produced during crack propagation were monitored during each test using commercially-available LOCAN-AT data aquisition equipment. A stainless steel waveguide with conical terminations was used to conduct the AE signals from the specimen to the transducer. Use of such a waveguide system has previously been shown not to affect the size distribution of AE events (Meredith & Atkinson 1983). The transducer used showed a flat response curve between 300 kHz and 1 MHz, and is as broad band as possible with a readily available commercial system. The parameters recorded for each acoustic emission event were its duration, peak amplitude, threshold crossing counts and energy (Pollock 1988), as well as time of event and load. A fixed threshold was established for each individual test depending on the background noise level. This ranged from 29 to 50 dB and was largely determined by the presence or absence of water. The level of background noise increased considerably when the specimen and waveguide were immersed in water, due to vibrations from the servo-system transmitted through the water. The only solution with the present experimental set up was to raise the threshold, thus unavoidably reducing the amount of data recorded during the wet tests.

Definition of the seismic b*-value*

The most useful way to quantify the scale-invariance of the AE seismicity is to use the Gutenberg–Richter relation, first defined for earthquake magnitude–frequency distributions (Gutenberg & Richter 1954):

$$\log N = a - bm, \tag{4}$$

where N is the number of earthquake events of a size greater than or equal to magnitude m, a is a constant and b is the seismic b-value. This equation can be fitted either to discrete or cumulative frequency plots, and may break down at higher magnitudes due to the finite moment release rate or the finite width of the seismogenic crust (Main & Burton 1986). Equation (4) may be applied to AE data to produce an AE b-value, once a correction factor of 20 has been introduced to allow for the fact that the AE amplitudes are measured in decibels (dB) whereas the Richter magnitude is defined in terms of the logarithm of a peak amplitude.

Figure 3 shows two amplitude–frequency distributions (discrete and cumulative) from one dry and one wet test that were both run at the same slow displacement rate of 0.016×10^{-6} m s^{-1}. The controlling variable here is the presence or absence of water. Both

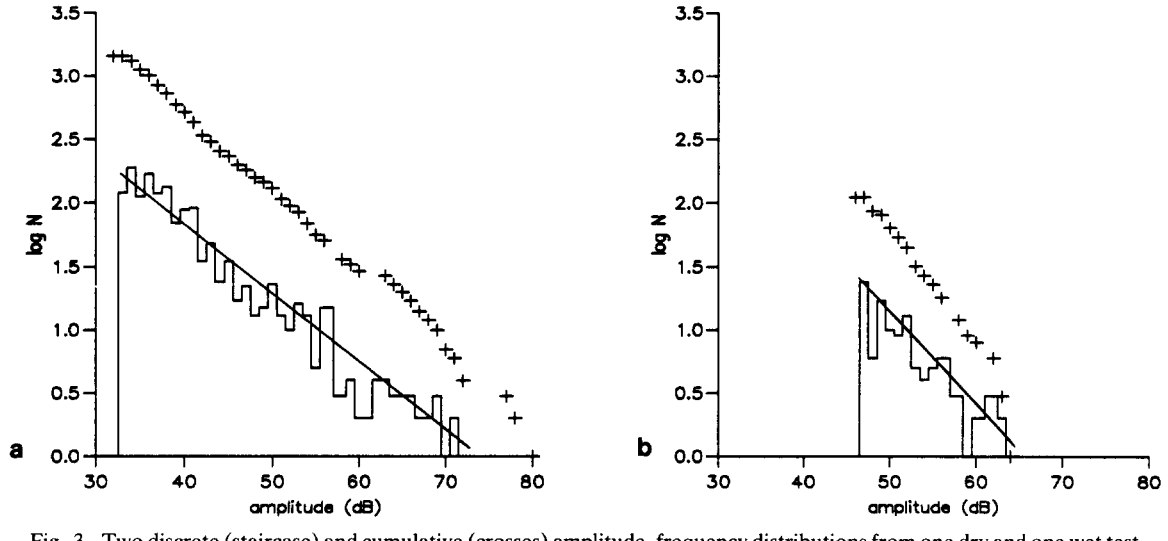

Fig. 3. Two discrete (staircase) and cumulative (crosses) amplitude–frequency distributions from one dry and one wet test, run at the same slow displacement rate of 0.016×10^{-6} m s^{-1}. The amplitude of the event measured in dB is equivalent to the earthquake magnitude after a correction factor of 20 is applied. It follows that the negative slope of this power-law distribution gives an AE b-value. (a) Distribution from a test run in dry air. The slope is relatively low (1.08 ± 0.04). This data gives an AE b-value of 1.41 ± 0.08 using the maximum likelihood method (Aki 1965), the error is expressed at the 66% confidence level or approximately one standard error. (b) Distribution from a test where the specimen was submerged in water. Even though much less data was collected due to the higher threshold used during the test to cut out the excessive background noise, the data still shows a much higher slope (1.49 ± 0.17), and b-value of 1.95 ± 0.21 from maximum likelihood method (Aki 1965).

plots illustrate the log-linear relationship of this distribution, indicating the similarity of the microseismicity of the double torsion tests with actual larger scale earthquake seismicity (as illustrated in Fig. 1b). The discrete data of Fig. 3(a), from the dry test has a negative slope of 1.08 ± 0.04. In comparison, Fig. 3(b) is from the wet test and has a higher slope of 1.49 ± 0.17 from the discrete data. Thus the effect of the fluid presence is to produce a greater relative proportion of smaller seismic sources.

The maximum likelihood method (Aki 1965) was chosen as the method of calculating the AE b-value during the time interval of constant stress intensity for each test. This method assigns an equal weighting to each recorded event, and reduces to the formula:

$$b = \frac{20 \log_{10} e}{\bar{a} - a_c}, \quad (5)$$

where b is the AE b-value, $\bar{a}$ is the mean amplitude in dB and a_c is the lower amplitude cut-off used in the calculation. The cut-off must be slightly greater than the threshold amplitude set during the experiment, since this electronic threshold represents a gradual rather than a sudden cut-off in reality. The b-values calculated using the maximum likelihood method ranged from 1.0 for the dry tests run at high stress intensity to 2.3 for the tests carried out at low stress intensity or higher fluid content.

STRUCTURAL ANALYSIS

The main advantage of the double torsion test is that the specimen geometry is ideal for inspection of the open tensile microfracture system produced. After each experiment a dye penetrant was applied to the polished undersurface of the specimen to enhance the visibility of the microfractures around the main crack. The undersurface of the central third of the specimen, representing the part which fails in pure mode I fracture at constant stress intensity, was then photographed using a photomicroscope, and the fracture patterns traced. Figure 4 shows examples of parts of two fracture patterns from different test specimens that were run at the same low

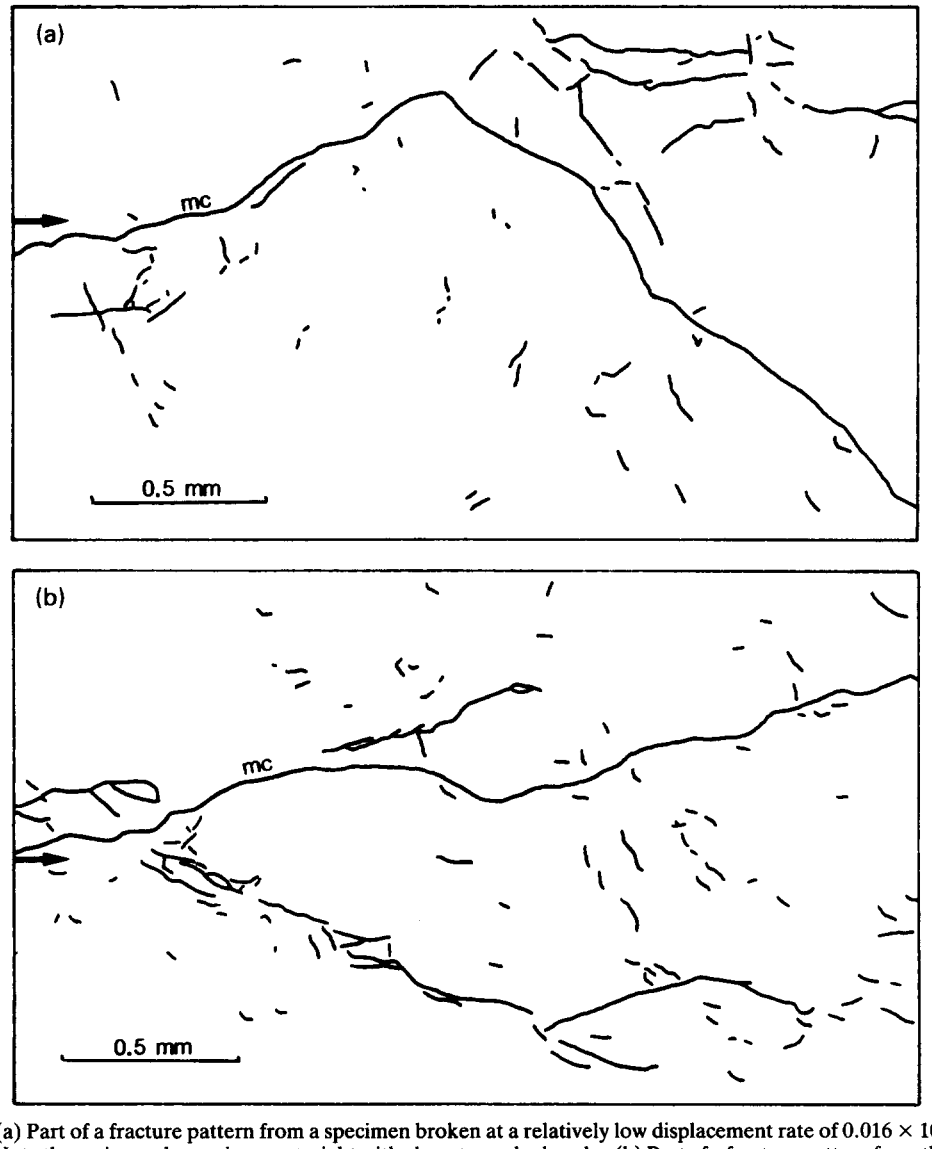

Fig. 4. (a) Part of a fracture pattern from a specimen broken at a relatively low displacement rate of 0.016×10^{-6} m s^{-1} in dry air. Note the main crack, **mc**, is very straight with abrupt angular breaks. (b) Part of a fracture pattern from the specimen of a wet test run at the same displacement rate as the example in (a). Note the main crack is much less angular and irregular.

displacement rate of 0.016×10^{-6} m s^{-1} (the AE data from these tests is illustrated in Fig. 3). The arrow indicates the direction of crack propagation. Figure 4(a) is from a specimen broken in 'air-dry' conditions. The main crack, marked **mc**, where the specimen broke in two, is seen to comprise relatively straight segments with abrupt angular breaks, or jogs, between segments. This is a general feature of the specimens that were tested dry, and ties in with the previous work described in the introduction. These macrocracks were predominantly transgranular in nature. There is significant subsidiary microcracking ahead of the jog point in this fracture pattern. Otherwise there is relatively little microcracking (the number of microcracks in this tracing is 148). It is useful to note that this test also produced a relatively low seismic b-value calculated by the maximum likelihood method (1.41 ± 0.16, the error is at the 90% confidence level—Aki 1965—i.e. 2 SDs).

This may be contrasted with the fracture pattern shown in Fig. 4(b) which is typical of the specimens broken in water. This test was run at the same displacement rate as the example in Fig. 4(a), but it can be seen here that the main crack is much less angular, but is more irregular due to intergranular cracking. The fracture pattern is characterized by a series of nascent bifurcations, that produce a wider damage zone around the macrocrack, and much more subsidiary microcracking (the number of microcracks in this tracing is 175). This also matches previous qualitative observations of stress corrosion cracking (Meredith & Atkinson 1983, Main *et al.* 1990). This test produced a relatively high AE b-value of 1.95 ± 0.42.

Therefore, the qualitative descriptions of the differences between the wet and dry fracture geometries appear to confirm the importance of fluid presence on the structure, as well as the scaling properties of the resulting seismicity.

Fractal geometry

As described in the introduction, a fractal dimension may be defined if a system is in some sense scale invariant and shows a power-law size distribution. From equation (1) we have:

$$\log N(L) = \text{constant} - D \log L \qquad (6)$$

and so by plotting log N vs log L, i.e. a crack length–frequency distribution, we obtain an area 'fractal' dimension D for the fracture pattern from the negative straight line slope of the distribution. For example, Fig. 1(a) shows $D = 1.76$ for the active faults in the United States (after Shaw & Gartner 1986).

In our case we are dealing with tensile microcracks which are relatively rough. We define the microcrack length in terms of a straight line drawn from tip to tip, (using the approximation that the crack is a straight elliptical fracture and small-scale variations in surface topography are not important). Although this method will underestimate the Hausdorff–Besicovitch dimension, it has the advantage of focusing attention on the overall population of cracks rather than the typical roughness of the major crack. The crack lengths are measured from the enlarged tracing to the nearest 0.5 mm and then converted to the actual size in microns by a multiplier of 11.428 (obtained from the size of the microscope field of view and photograph size).

Figure 5 shows both the discrete and cumulative length–frequency distributions of the two fracture patterns of Fig. 4. At progressively smaller crack lengths, the discrete data are seen to peak and then reduce. The most likely explanation is that the data are simply incomplete due to undercounting of the cracks that are not visible or have not reached the surface. A minimum value for the crack length (L_{min}) representing a real or experimentally-controlled lower fractal limit must

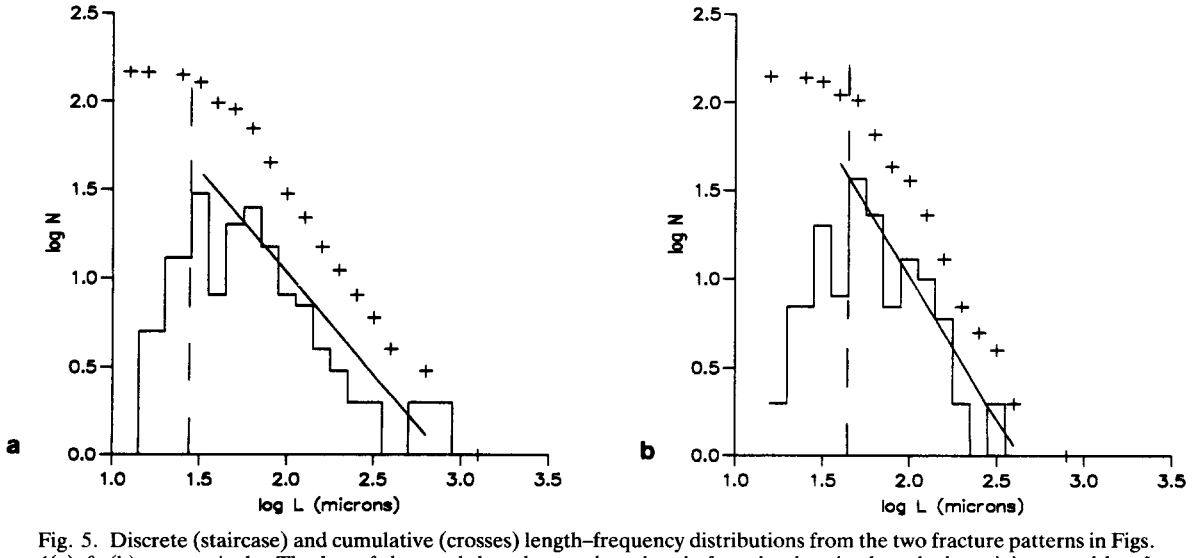

Fig. 5. Discrete (staircase) and cumulative (crosses) length–frequency distributions from the two fracture patterns in Figs. 4(a) & (b), respectively. The log of the crack length must be taken before the data is plotted, thus giving equal log L histogram bin sizes. Excluding cracks of length < L_{min} microns, both plot as approximately straight line power-law distributions where the negative straight line gives the exponent D. (a) Length–frequency plot from the air dry test. This slope is relatively low, and has $D = 1.16 \pm 0.14$, where the error is given as one standard error. (b) The distribution from the slower wet test gives a higher slope and $D = 1.56 \pm 0.18$.

Table 1. Summary of experimental results

Test	V ($\times 10^{-6}$ m s^{-1})	K_I/K_{IC}	b	$N(b)$	D	$N(D)$
Dry						
0022	6.9	0.65	1.41	295	1.16	70
0104	7.4	0.68	1.31	3379	—	—
0102*	24.0	0.64	1.35	2562	1.54	780
0006	66.0	0.77	1.61	143	1.42	98
0007	56.8	0.82	1.32	813	—	—
0101	66.0	0.61	1.26	627	—	—
0024	670.0	0.87	1.12	2314	1.02	91
0055*	568.0	0.77	1.19	802	1.41	353
0110	640.0	0.71	1.25	924	—	—
0111	1820.0	0.81	1.06	1391	—	—
Damp						
0052	707.0	0.68	1.59	189	—	—
Wet						
0051*	7.04	0.64	1.95	81	1.71	712
0118	21.3	0.64	1.96	27	—	—
0028	62.6	0.71	1.61	90	1.24	131
0117	89.0	0.70	1.75	121	—	—
0037	170.0	0.73	1.99	82	1.66	177
0035	660.0	0.68	1.24	125	1.06	69
0036	638.0	0.67	1.84	130	1.37	104
0040	550.0	0.76	1.62	34	—	—
0116	637.0	0.73	1.43	45	—	—
0041*	1770.0	0.77	1.42	197	1.63	530
0119	2440.0	0.71	1.85	42	—	—

*Obtained from several summed data sets.

therefore be introduced, and the data below this disregarded in the calculation of the exponent D. L_{min} varies only slightly in each of the fracture patterns investigated here, and has a typical value of 30 μm. Above L_{min} both distributions plot as parallel straight lines on the log–log axes, indicating the expected power law relation in both discrete and cumulative statistics. The fractal range (L_{min} to L_{max}) is typically 1–1.5 orders of magnitude. The length distribution exponent D may be estimated from the gradient of the reduced major axis of this distribution (Williams 1986), given by:

$$D = \frac{\mathrm{SD}(\log N)}{\mathrm{SD}(\log L)}, \tag{7}$$

where SD is the standard deviation. A maximum likelihood fit was found to be too sensitive to the relatively subjective choice of a lower cut-off, and in this case the gradient calculation was found to be a more robust measurement of D.

Using this error bound, Fig. 5(a), from the air-dry test, gives a relatively low slope and a length distribution exponent D of 1.6 ± 0.14 (where the error is given as one standard error). However, Fig. 5(b) from the wet test appears to have a relatively higher slope, giving $D = 1.56 \pm 0.18$. This implies that there is a greater relative number of smaller cracks in the latter case, due to the activation of the stress corrosion mechanism. The length distribution exponent D may therefore be used, together with its error bound, to compare the fracture geometries in a quantitative and objective way.

It should be noted that each individual fracture pattern represents only a small proportion (1.5–2 mm) of the specimen length (of 50 mm) due to the scale of the microfractures, and hence the data sets are rather small. Several fracture patterns were taken from some specimens to produce a summed length distribution exponent from an increased data set. This process did not produce exponents that differed significantly from those obtained from the smaller data sets, and so was limited in order to examine as many specimens as possible.

SYNTHESIS OF RESULTS

Given the quantitative bounds on the data discussed above, we can now examine crack growth under different environmental conditions and the resulting scaling of crack structure and seismicity. Table 1 contains a summary of the results obtained from the present experimental series. The length distribution exponents that were obtained from several summed data sets are marked with an asterisk. Several repeat tests carried out in the same environmental conditions indicate a good repeatability of results.

Relation of seismic scaling to the physics and chemistry of subcritical crack growth

The experimental control parameters of each test may be correlated with the seismic data recorded during the test in the form of a plot of the stress intensity acting during the time period of constant K_I, against the average AE b-value calculated from the acoustic emissions monitored during the same period. Figure 6 is a summary diagram of K_I/K_{IC}, i.e. the stress intensity normalized by the mode I fracture toughness K_{IC} ($K_{IC} = 2.9$ for

the Loch Uisg microgranodiorite) vs AE b-value. Each data point on the diagram represents a single test. As already mentioned, two different lower cut-off amplitudes were used in calculating the b-values for the wet and dry tests to reduce the error in b. It should be noted that if the same value ($a_c = 48.5$) is used for all the tests, the major characteristics of the b vs K_I/K_{IC} plot do not change, apart from introducing more scatter into the dry test results.

Several observations may be made from Fig. 6. The data are observed to divide into two populations on the basis of fluid content. The wet tests run at a low displacement rate, i.e. low crack velocity, with H_2O present in the environment of the crack tip, plot in the low K_I, high b region of the graph. Wet tests run at a high displacement rate plot with higher K_I, lower b. Air-dry tests, with no fluid present, run at high displacement rates also plot with high K_I, low b. However, dry tests run at lower displacement rates plot in the low K_I, low b region. Correlation slopes may be drawn independently for the wet and dry populations. These are both seen to be negative; the 'dry' slope has a gradient of -1.3 ± 0.3 (with a significant negative correlation coefficient $r = -0.6$); the 'wet' slope has a higher gradient of -4.5 ± 1.0 (where $r = -0.6$). The two slopes converge at around $K_I/K_{IC} = 0.85$, $b = 1.1$. The test that was run in 'damp' conditions as an intermediate case plots between these two populations.

Tests run at low displacement rates, with low stress intensities, i.e. those promoting slow subcritical crack growth, show a first-order effect of fluid presence. The wet tests give high seismic b-values indicating many small AE events, suggesting that the effect of stress corrosion is to produce a distributed array of smaller microcracks. In contrast, the dry tests give low b-values, indicating a higher proportion of large to small events when there is a smaller quantity of active chemical agent present to initiate stress corrosion reactions. Thus more of the overall crack growth is concentrated on the largest cracks.

Tests run at high displacement rates, with high crack velocities and high K, show less difference between the wet and dry tests. Both give lower b-values suggesting that even if fluid is present there is less time for stress corrosion reactions to occur at the crack tip as crack growth is more dynamic. The physical movement of fluid to the crack tip is also likely to be limited by the high velocity of rupture at the tip near to K_{IC}. The convergence of the correlation lines at high K_I indicates that the mechanism of crack propagation is highly sensitive to fluid presence and environmental conditions at low K_I, and less obviously at higher K_I and dynamic fracture velocities.

Two important conclusions can be made from Fig. 6. First, the presence of an active fluid at the crack tip has a first-order influence on seismicity during tensile fracture. Second, the b-value correlates negatively with stress intensity, suggesting that at higher stress concentrations there is a higher proportion of larger seismic sources. These results are consistent with previous work using the double torsion relaxation method (Meredith & Atkinson 1983, Main *et al.* 1990).

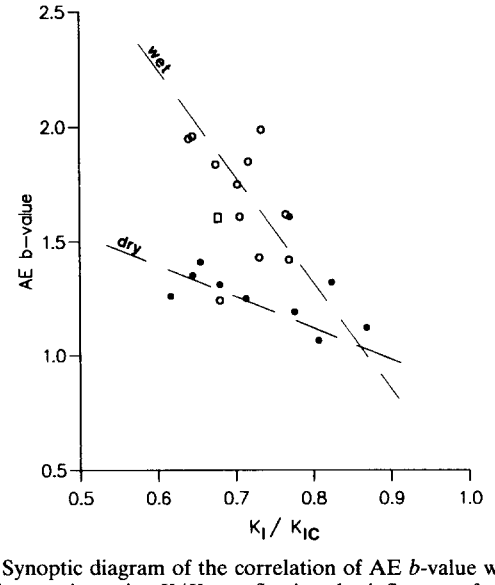

Fig. 6. Synoptic diagram of the correlation of AE b-value with normalized stress intensity K_I/K_{IC}, reflecting the influence of crack tip humidity during tensile crack propagation. These data are from a new series of double torsion tests run at various constant displacement rates, in ambient temperature and pressure, on specimens of Loch Using microgranodiorite. Solid circles, air-dry tests; open box, 'damp' test; open circles, wet tests. The dashed lines are the best fits to the data points, and converge at approximately $K_I/K_{IC} = 0.85$ and $b = 1.1$. The 'dry' slope has a negative gradient of 1.32 ± 0.31 (one standard error), with a correlation coefficient $r = -0.59$ indicating a significant correlation. The 'wet' slope has a negative gradient of 4.49 ± 1.03 and $r = -0.6$.

Relation of structure to seismicity at microfracture scale

As described in the previous sections, for each double torsion test we have two independent quantitative measurements reflecting (a) the scaling of the seismicity associated with crack growth during the test (the AE b-value), and (b) the structure left in the specimen after the test (the length distribution exponent, D). Figure 7 shows a plot of the AE b-value, calculated by the maximum likelihood method (Aki 1965), vs the exponent D, calculated from the gradient of the reduced major axis of the straight-line length distribution. Several typical error bars (of one standard error to either side of the data point) are included, showing the systematically higher errors in b-value associated with the wet tests. In general the wet test specimens show high D as well as high b, indicating a higher ratio of small to large cracks, suggesting that the presence of the active environmental agent and fluid–rock interaction is affecting the structure as well as the seismicity during crack growth.

Overall, a positive correlation between D and b is apparent from this plot, as predicted from equation (2), although there is a large scatter due to: the relatively small number of cracks which could be reliably imaged optically; the difficulties in maintaining a constant stress intensity at the crack tip; and the problem with background noise encountered during the wet tests. To test the correlation, Pearson's product–moment correlation

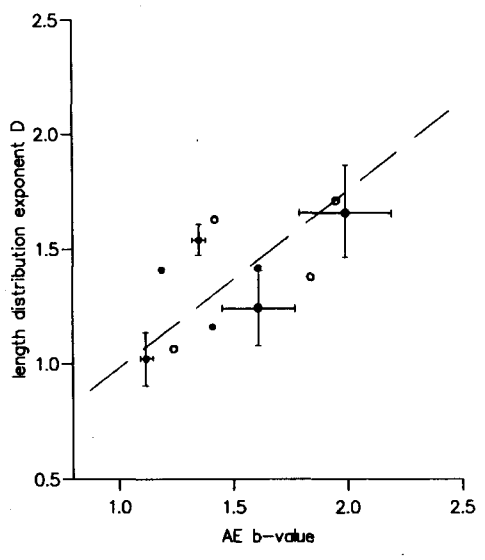

Fig. 7. Correlation of the AE b-value with the length distribution exponent D. Both parameters were measured from the same double torsion specimen. Solid circles, dry tests; open circles, wet tests. Several typical error bars of one standard error to either side of the data point are shown. The dashed line represents the reduced major axis of D with b, giving a gradient of 0.78 ± 0.18 and intercept of 0.18 ± 0.28; the correlation coefficient $r = 0.71$.

coefficient, r, of D with b was found to be 0.71 (perfect positive correlation gives $r = 1$; no correlation, $r = 0$), indicating that the positive correlation is statistically significant. Therefore, a straight line may be drawn on the b vs D plot of Fig. 7, thus giving a gradient and intercept for the relationship. The gradient of the reduced major axis is found to be 0.78 ± 0.18, and the intercept to be 0.18 ± 0.28 so that:

$$D = 0.78b + 0.18. \quad (8)$$

Therefore the length distribution exponent obtained from the structure is positively correlated with the AE b-value. Equation (8) approximates within its error bounds to a straight line of slope just less than 1.0 passing near to the origin, similar to equation (2) if c is assumed to be 3 in the case of the experimental results (Main *et al.* 1989). However, it must be remembered that the exponent D is a measure from the analysis of the visible cracks on the polished surface, i.e. a two-dimensional slice, whereas b represents the microseismicity from the three-dimensional specimen. This complication is discussed further below.

Discussion

Although we have shown a statistically significant positive relation between the length distribution exponent D and the AE b-value, it should not be expected that the two-dimensional (areal) exponent D_A should show a one to one correspondence with the three-dimensional (volume) exponent D_V, and consequently this will affect its precise relation with b. However, we would expect D_V and D_A to be positively correlated (Heffer & Bevan 1990). In all cases, we would expect $D_V \geq D_A$ by definition. For ideal, self-similar fractal objects formed by a deterministic algorithm, $D_V = D_A + 1$ (Mandelbrot 1982), but it is clear that this simple relation does not hold in general for the power-law exponent of fault and fracture length distributions. For example, it is observed that $1 < D_V < 3$ (Main *et al.* 1990), whereas $D_A > 1$ by definition for the case of the one-dimensional interception on a two-dimensional surface for a fractal array of cracks. In particular, the condition for dynamic failure is marked by $D = 1$, both in direct observation of throughgoing fault systems and as inferred from the b-value of foreshock sequences (Main *et al.* 1990). If the more general correlation is linear and positive, then:

$$D_V = \alpha D_A + \phi, \quad (9)$$

where $\alpha = 1.0$ and $\phi = 1.0$ for deterministic fractals. This may be applied to equation (2), so that the predicted relationship between the b-value and the area exponent measured on the polished surface is:

$$D_A = \frac{3b}{\alpha c} - \frac{\phi}{\alpha}. \quad (10)$$

Thus equation (8) may be interpreted with respect to the generalized equation (10). From equation (10), where $3/(\alpha c)$ = slope and $-\phi/\alpha$ = intercept, and assuming $c = 3$, we find $\alpha = 1.28$ and $\phi = 0.23$. Therefore, we can compare these results to the inferred volume fractal dimension D_V by:

$$D_V = 1.28D_A - 0.23. \quad (11)$$

This gives $D_V > D_A$ for $D_A > 0.82$, but not in the manner suggested by deterministic fractals. The difference may arise because of mode I cracking being concentrated on the free polished surface in the double torsion loading arrangement. Microcracks will then tend to preferentially grow into the plate from the initial flaws on the free surface. The upper surface also fails in tension, but with a slightly lower stress intensity, and will tend to have preferentially less mode I cracking. This might imply that the fractal scaling is self-affine (i.e. different in different directions) rather than self-similar, with D_A varying from a maximum on the polished under surface, to a minimum on the upper surface, and with the smallest microcracks preferentially confined to the outer surface with the greatest mode I stress concentration and greater fluid presence.

If c is different from our estimate then we would expect different ranges for D_V: for $c = 1.5$, $3.02 < D_V < 5.58$; and for $c = 1$, $4.54 < D_V < 8.39$. These values of c produce unacceptably high inferred values of D_V, which proves self-consistency at least. There is no value of c consistant with the self-similar scaling of deterministic fractals.

An additional complication may arise if seismic moment does not scale with length cubed, for example for seismic sources large compared to the specimen thickness (cf. the finite seismogenic depth in the brittle crust). In the general case we might have $M_0 \propto L^\eta$, so that the slope of equation (8) would be equal to $\eta/\alpha c$, where η need not necessarily be equal to 3. This discussion

highlights the importance of establishing the seismic scaling exponents η and c independently in future studies. This would require more accurate, broad-band recording of the seismic sources, as well as accurate determination of source locations and path effects between the seismic source and the receiver.

Thus, although we have established a definite positive correlation between b and D_A, and between D_A and D_V, we cannot at present be more precise about the relationship between D_A and D_V than in the preceding discussion, other than to urge a note of caution in scaling results from borehole or surface mapping to volume deformation.

CONCLUSIONS

This experimental study has provided new data which will help establish the nature of the relationship between the evolution of brittle structure and seismicity. The following conclusions are confirmed.

(i) The AE b-value correlates negatively with the normalized stress intensity K_I/K_{IC}. This implies that the greater the stress concentration, the greater the relative proportion of larger seismic sources.

(ii) Fluid presence has a first-order influence on seismicity during tensile crack growth, because of activation of the stress corrosion mechanism. The greater the fluid–rock interaction, the greater the relative proportion of smaller seismic sources.

The following conclusions are specific to the present work.

(i) The crack length distribution exponent D can be a suitable diagnostic quantitative measure of differences in fractal scaling and the structure of tensile microfracture during subcritical crack growth under different conditions.

(ii) Fluid presence has a first-order effect on this structural scaling during tensile microfracture, producing a greater relative proportion of smaller cracks, compared to the number produced in dry conditions.

(iii) The 'fractal' dimension D from the crack length distribution correlates positively with the b-value, as predicted from a simple dislocation model of the seismic source. This confirms the applicability of such scaling laws in modelling the evolution of fault growth over integrated increments of displacement and fault extension.

Acknowledgements—We thank R. F. Cheeney for help in collecting and preparing rock samples and advice on statistics, and Chris Stuart for providing programs for acoustic emission analysis. Thanks must also go to Patience Cowie for helpful suggestions, and Chris Barton and one anonymous reviewer for their constructive comments. Financial support was provided by the Natural Environment Research Council through a research studentship for CGH (award GT4/89/GS/033) and a research grant for IGM and PGM (grant GR/6812).

REFERENCES

Aki, K. 1965. Maximum likelihood estimates of b in the formula $\log N = a - bm$ and its confidence limits. *Bull. Earthquake Res. Inst., Tokyo Univ.* **43**, 237–239.

Aki, K. 1981. A probabilistic synthesis of precursory phenomena. In: *Earthquake Prediction: An International Review* (edited by Simpson, D. W. & Richards, P. G). *Am. Geophys. Un. Maurice Ewing Ser.* **4**, 566–574.

Anderson, O. L. & Grew, P. C. 1977. Stress corrosion theory of crack propagation with application to geophysics. *Rev. Geophys. & Space Phys.* **15**, 77–104.

Atkinson, B. K. 1982. Subcritical crack propagation in rocks: theory, experimental results and applications. *J. Struct. Geol.* **4**, 41–56.

Atkinson, B. K. 1987. Introduction to fracture mechanics and its geophysical applications. In: *Fracture Mechanics of Rock* (edited by Atkinson, B. K.). Academic Press, London. 1–26.

Charles, R. J. 1958. Static fatigue of glass. *J. Appl. Phys.* **29**, 1549–1560.

Cowie, P. A. & Scholz, C. H. 1992a. Physical explanation for displacement-length relationship for faults using a post-yield fracture mechanics model. *J. Struct. Geol.* **14**, 1133–1148.

Cowie, P. A. & Scholz, C. H. 1992b. Relationship between scaling laws for earthquakes and the growth of faults by accumulation of seismic slip. *J. geophys. Res.* **97**, 11,085–11,096.

Das, S. & Scholz, C. H. 1981. Theory of time-dependent rupture in the earth. *J. geophys. Res.* **86**, 6039–6051.

Etheridge, M. A. 1983. Differential stress magnitudes during regional deformation and metamorphism: upper bound imposed by tensile fracturing. *Geology* **11**, 231–234.

Fuller, E. R. 1979. An evaluation of double torsion testing—analysis. In: *Fracture Mechanics Applied to Brittle Materials. ASTM, STP* **678**, 3–18.

Gutenberg, B. & Richter, C. F. 1954. *Seismicity of the Earth and Associated Phenonena* (2nd edn). Princeton University Press, Princeton, New Jersey.

Heffer, K. J. & Bevan, T. G. 1990. Scaling relationships in natural fractures—data, theory and applications. *Soc. Petrol. Engrs.* SPE 20981.

Kanamori, H. & Anderson, D. L. 1975. Theoretical bases of some empirical relations in seismology. *Bull. seism. Soc. Am.* **65**, 1073–1095.

King, G. C. P. 1983. The accommodation of large strains in the upper lithosphere of the earth and other solids by self-similar fault systems: the geometrical origin of b-value. *Pure & Appl. Geophys.* **121**, 761–815.

Kerrich, R., La Tour, T. E. & Barnet, R. L. 1981. Mineral reactions participating in intragranular fracture propagation: implications for stress corrosion cracking. *J. Struct. Geol.* **3**, 77–87.

Main, I. G. & Burton, P. W. 1984. Information theory and the earthquake frequency-magnitude distribution. *Bull seism. Soc. Am.* **74**, 1409–1426.

Main, I. G. & Burton, P. W. 1986. Long term earthquake recurrence constrained by tectonic seismic moment release rates. *Bull seism. Soc. Am.* **76**, 297–304.

Main, I. G., Meredith, P. G. & Jones, C. 1989. A reinterpretation of the precursory seismic b-value anomaly using fracture mechanics. *Geophys. J.* **96**, 131–138.

Main, I. G., Meredith, P. G., Sammonds, P. R. & Jones C. 1990. Influence of fractal flaw distributions on rock deformation in the brittle field. In: *Deformation Mechanisms, Rheology and Tectonics* (edited by Knipe, R. J. & Rutter, E. H.). *Spec. Publs geol. Soc. Lond.* **54**, 81–96.

Mandelbrot, B. B. 1982. *The Fractal Geometry of Nature*. W. H. Freeman, San Francisco.

Marrett, R. & Allmendinger, R. W. 1990. Kinematic analysis of fault slip data. *J. Struct. Geol.* **12**, 973–986.

Marrett, R. & Allmendinger, R. W. 1991. Estimates of strain due to brittle faulting: sampling of fault populations. *J. Struct. Geol.* **13**, 735–738.

Meredith, P. G. 1983. A fracture mechanics study of experimentally deformed crustal rocks. Unpublished Ph.D. thesis, University of London.

Meredith, P. G. & Atkinson, B. K. 1983. Stress corrosion and acoustic emission during tensile crack propagation in Whin Sill dolerite and other basic rocks. *Geophys. J. R. astr. Soc.* **75**, 1–21.

Meredith, P. G. & Atkinson, B. K. 1985. Fracture toughness and subcritical crack growth during high-temperature tensile deformation of Westerly granite and Black gabbro. *Phys. Earth & Planet. Interiors* **39**, 33–51.

Meredith, P. G., Main, I. G. & Jones, C. 1990. Temporal variations in seismicity during quasi-static and dynamic rock failure. *Tectonophysics* **175**, 249–268.

Pollock, A. A. 1988. Practical guide to acoustic emission. In: *LOCAN-AT Handbook*. Physical Acoustics Corp., U.S.A.

Shaw, H. R. & Gartner, A. E. 1986. On the graphical interpretation of palaeoseismic data. *U.S. geol. Surv. Open-file Rep.* **86–394**.

Scholz, C. H. & Cowie, P. A. 1990. Determination of geologic strain from fault slip data. *Nature* **346**, 837–839.

Segall, P. & Pollard, D. D. 1983. Joint formation in the granitic rock of the Sierra Nevada. *Bull. geol. Soc. Am.* **94**, 563–575.

Turcotte, D. L. 1989. Fractals in geology and geophysics. *Pure & Appl. Geophys.* **131**, 171–196.

Walsh, J., Watterson, J. & Yielding, G. 1991. The importance of small scale faulting in regional extension. *Nature* **351**, 391–393.

Turcotte, D. L. 1992. *Fractals and Chaos in Geology and Geophysics*. Cambridge University Press, Cambridge.

Walsh, J. & Watterson, J. 1992. Populations of fault displacements and their effects on estimates of fault-related regional extension. *J. Struct. Geol.* **14**, 701–712.

Williams, D. P. & Evans, A. G. 1973. A simple method for studying slow crack growth. *J. T. Eval.* **1**, 264–270.

Williams, R. G. B. 1986. *Intermediate Statistics for Geographers and Earth Scientists*. Macmillan, London.